

## **Mode II fracture mechanics properties of solid wood measured by the three-point eccentric end-notched flexure test**

(Abbreviated title: Three-point eccentric end-notched flexure test of solid wood)

Hiroshi Yoshihara\*

Faculty of Science and Engineering, Shimane University, Nishikawazu-cho 1060,  
Matsue, Shimane 690-8504, Japan

\* Corresponding author. Tel: +81-852-32-6508; fax: +81-852-32-6123.

*E-mail address:* yosihara@riko.shimane-u.ac.jp

### **Abstract**

A three-point eccentric end-notched flexure test was conducted using specimens of western hemlock to determine the fracture mechanics properties under Mode II conditions while extending the crack length range for stabilising the crack propagation. The location of the loading point was varied during the test, and the effect of the loading point location on the initiation and propagation fracture toughness values was examined. With the proposed method, fracture mechanics properties were appropriately obtained at greater crack propagation lengths than in the conventional three-point end-notched flexure test when the loading point was not extremely close to the supporting point at the crack-free region.

**Keywords:** three-point eccentric end-notched flexure test; solid wood; initiation fracture toughness; propagation fracture test; resistance curve

## 1. Introduction

When a crack propagates in a fibrous material such as solid wood, the fracture toughness often increases as the crack length increases because of the existence of a fracture process zone (FPZ) ahead of the crack tip and fibre bridgings between the crack surfaces. Therefore, the fracture mechanics properties of fibrous materials including solid wood have often been evaluated by a resistance curve (*R*-curve) that is typically determined from the relationship between the fracture toughness and the crack length increment during the crack propagation. A three-point end-notched flexure (3ENF) test is a simple method for determining Mode II fracture mechanics properties such as the initiation fracture toughness and the *R*-curve. In recent conventional 3ENF tests where the load is applied to the mid-span, the fracture mechanics properties have been frequently mathematically defined according to beam theory [1-12]. When measuring the *R*-curve, however, the 3ENF test has a drawback in that the ratio of the initial crack length to the half span should be greater than 0.7 to stabilise the crack propagation. To obtain information on the fracture mechanics properties, it is desirable to obtain the

*R*-curve by stabilising the crack propagation length over a wide range. Several methods such as stabilised end-notched flexure (SENF), end-loading shear (ELS), tapered end notched flexure (TENF), over-notched flexure (ONF), and four-point bend end-notched flexure (4ENF) tests have been used to stabilise crack propagation over a range wider than the 3ENF test [13-25]. Nevertheless, there are several disadvantages in these methods, even though they are effective at stabilising crack propagation. A SENF test requires a servo valve-controlled testing machine that is often complicated to control [13]. The testing data in an ELS test can often vary according to the clamping conditions [14, 15]. The equation for deriving the fracture toughness in the TENF test is more complicated than that of a 3ENF test [16]. In an ONF test, the effect of the frictional forces between the crack surfaces is very significant and continuously increases the *R*-curve during crack propagation [17-19]. The 4ENF test may be superior to the aforementioned methods because of its simplicity and stability in crack propagation [14, 20-25]. To apply a 4ENF test to solid wood, however, it is often difficult to let the crack propagate while preventing the specimen failure by bending at the loading point in the cracked portion without cutting deep grooves in both

side-surfaces [23, 24]. In fact, there are few examples of applying a 4ENF test to solid wood. It is more convenient to measure the *R*-curve over a wide range of propagation crack lengths through simple procedures such as equipment and specimen preparation.

In a conventional 3ENF test in which the load is applied at the mid-span of the specimen, the range of the crack length enabling stable propagation is theoretically restricted from 0.35 to 0.5 times the span. This range can be easily extended without preparing any special equipment or specimens with a three-point eccentric end-notched flexure (3EENF) test, the details of which are demonstrated below.

This study conducted a 3EENF test on western hemlock specimens to obtain an *R*-curve, defined as the relationship between the propagation fracture toughness and the propagation crack length, was obtained. Based on the *R*-curve, Mode II initiation fracture toughness and represented value of the propagation fracture toughness, defined as the averaged value of the propagation fracture toughness at the plateau portion of the *R*-curve. The location of the loading point was varied in the 3EENF test, and the effect of the location on the fracture mechanics properties described above was examined.

## 2. Three-point eccentric end-notched flexure analyses

Fig. 1 shows a diagram of the three-point eccentric end-notched flexure (3EENF) test for the Mode II analysis. A specimen with a width of  $B$ , a depth in the cracked portion of  $H$  and a crack length of  $a$ , is supported by a span with a length of  $2L$ . As shown in the figure, a load of  $P$  is eccentrically applied and the distance between the loading point and the supporting point at the cracked portion is defined as  $c$ . By solving the equation of flexure while considering the transverse shear force, the load-deflection compliance,  $C_L$ , is given as:

$$C_L = \frac{d}{P} = \frac{(2L - c)^2 (3a^3 + 2c^2L)}{8E_x B H^3 L^2} + \frac{s(2L - c)}{4G_{xy} B H L} \quad (1)$$

where  $E_x$  is the Young's modulus in the length direction, which is defined as the  $x$ -direction,  $G_{xy}$  is the shear modulus in the length/depth plane, which is defined as the  $xy$ -plane,  $s$  is the Timoshenko's shear factor which is equal to 1.2 for the beam with a rectangular cross-section, and  $\delta$  is the deflection at the loading point. Therefore, the Mode II energy release rate,  $G_{II}$ , is derived as:

$$G_{II} = \frac{P^2}{2B} \frac{dC_L}{da} = \frac{9(2L - c)^2 P^2 a^2}{16E_x B^2 H^3 L^2} \quad (2)$$

Under constant loading point deflection condition,  $dG_{II}/da$  is derived from Eqs. (1) and

(2) as follows:

$$\frac{dG_{II}}{da} = \frac{9d^2(2L-c)^2 a}{8E_x B^2 H^3 L^2 C^2} \left( 1 - \frac{9a^3}{3a^3 + 2c^2 L} \right) \quad (3)$$

To stabilise the crack propagation,  $dG_{II}/da$  should be negative; thus,

$$a \geq \sqrt[3]{\frac{c^2 L}{3}} \quad (4)$$

Based on this equation, the minimum value of  $a/2L$ , defined as  $a_{\min}/2L$ , can be

determined from the loading point location relative to the span length  $c/2L$  as follows:

$$\frac{a_{\min}}{2L} = \sqrt[3]{\frac{1}{6} \left( \frac{c}{2L} \right)^2} \quad (5)$$

The path length where the crack stably propagates, defined as  $l_s$ , is derived as follows:

$$l_s = c - a_{\min} = 2L \left[ \frac{c}{2L} - \sqrt[3]{\frac{1}{6} \left( \frac{c}{2L} \right)^2} \right] \quad (6)$$

When the value of  $l_s$  is large, the  $R$ -curve can be obtained over a wide range of crack

propagation lengths. Fig. 2 shows the relationship between the values of  $l_s/2L$  and  $c/2L$

obtained from Eq. (6). In a conventional 3ENF test,  $c = 0.5$  so that  $l_s/2L = 0.15$ ; by

contrast,  $l_s/2L = 0.5$  in the most conventional 4ENF test [20-25]. Therefore, when the

loading point is located rightward of the mid-span, the range of the path length where

the crack stably propagates is wider than in a conventional 3ENF test, although it is narrower than that in a 4ENF test.

In an actual fracture test, the load-deflection compliance is often greater than that obtained by Eq. (2) because of the deformation caused by the transverse shear force, which is the second term in Eq. (1), the fracture process zone (FPZ) induced at the region ahead of the crack tip, and the fibre bridgings; the sample behaves as if the crack length value is longer than the actual value. To accommodate this phenomenon, Eqs. (1) and (2) are modified as [9]:

$$C_L = \frac{(2L - c)^2 [3(a + D)^3 + 2c^2L]}{8E_x BH^3 L^2} = \frac{(2L - c)^2 (3a_{eq}^3 + 2c^2L)}{8E_x BH^3 L^2} \quad (7)$$

$$G_{II} = \frac{9(2L - c)^2 P^2 a_{eq}^2}{16E_x B^2 H^3 L^2} \quad (8)$$

where  $\Delta$  is the correction value of the crack length, and  $a_{eq}$  is the equivalent crack length.

The influences of the transverse shear force, FPZ ahead of the crack tip, and fibre bridgings are contained in the  $a_{eq}$  value. Based on Eq. (7), the  $a_{eq}$  value can be obtained

as

$$a_{eq} = \left[ \frac{8E_x BH^3 L^2 C_L}{3(2L - c)^2} - \frac{2c^2L}{3} \right]^{\frac{1}{3}} \quad (9)$$

Once the value of  $G_{II}$  is obtained from Eq. (8), the  $E_x$  value must then be measured with a separate test. This obstacle can be reduced when measuring the strain at a specific point in the specimen during the fracture test. This data reduction method was originally proposed by the author as a “compliance combination method” and it may prove promising for the analysis of 3EENF test results [5, 9, 11, 23, 24]. According to elementary beam theory, the longitudinal strain at a loading point  $\varepsilon_x$  is derived as follows:

$$e_x = \frac{3(2L - c)cP}{4E_xBH^2L} \quad (10)$$

The  $\varepsilon_x$  value is not influenced from the transverse shear force [9, 26]. Therefore the load-strain compliance  $C_s$  can be obtained as follows:

$$C_s = \frac{e_x}{P} = \frac{3(2L - c)c}{4E_xBH^2L} \quad (11)$$

By using Eqs. (7) and (11), the Young’s modulus  $E_x$  can be eliminated and the  $a_{eq}$  value can be obtained as follows:

$$a_{eq} = \left( \frac{2HLc}{2L - c} \cdot \frac{C_L}{C_s} - \frac{2}{3}c^2L \right)^{\frac{1}{3}} \quad (12)$$

By substituting Eqs. (11) and (12) into Eq. (8),  $G_{II}$  can be obtained as

$$G_{II} = \frac{3(2L - c)C_S P^2}{4BHLc} \left( \frac{2HLc}{2L - c} \cdot \frac{C_L}{C_S} - \frac{2}{3}c^2L \right)^{\frac{2}{3}} \quad (13)$$

Using the compliance combination method, the  $G_{II}$  value can be solely evaluated by the fracture test without measuring the crack length or any elastic constants that are implicitly contained in the load-deflection compliance  $C_L$  and the load-longitudinal strain compliances  $C_S$ .

### 3. Finite element calculations

Two-dimensional finite element analyses (2D-FEAs) were independently conducted on the actual fracture tests detailed below to examine the validity of the 3EENF test. The ANSYS 12 program, which is available in the Shimane University library, was used for the FE analyses. Figs. 3(a) and (b) show the FE mesh used in the calculations and the boundary conditions corresponding to the 3EENF test simulations. The horizontal length of the model was 430 mm, and the model width,  $B$ , was 12 mm. The depth of the model,  $2H$ , was 24 mm. The model consisted of four-node plane

elements. The mesh was constructed to be finer closer to the crack tip, as shown in Fig. 3(b). The dimensions of the element at the delamination front were 0.5 and 0.5 mm in the  $x$ - and  $y$ -directions, respectively. Table 1 presents the elastic properties used in the present calculations, which were similar to those used in a previous study that used spruce specimens [11]. The initial crack length  $a_0$  was determined as  $c - l_s$ , thus theoretically confirming stable crack propagation in the fracture test. Table 2 shows the  $a_0$  value corresponding to the  $c/2L$  and  $c$  values.

The variation of the  $G_{II}$  value under the varying crack length  $a$  was examined in the FEAs. Table 3 shows the crack length  $a$  and the applied load  $P$  corresponding to the loading point  $c$ . The intervals of the  $a$  value were determined to be approximately equal to  $l_s/5$ , whereas the  $P$  value was determined to correspond to the  $G_{II}$  value in Eq. (2) as  $1000 \text{ J/m}^2$ , which was approximately equal to the propagation fracture toughness  $G_{IIR}$  obtained in a previous study [11]. The load-deflection compliance  $C_L$  was obtained from the displacement of the node at the point behind the loading point.

The  $G_{II}$  value was calculated using three data reduction methods: beam theory, compliance combination, and compliance calibration methods. In the beam theory

method, the  $G_{II}$  and  $a_{eq}$  values were obtained by substituting the  $E_x$  and  $P$  values shown in Tables 1 and 2 and the  $C_L$  value into Eqs. (9) and (8), respectively. In the compliance combination method, the  $G_{II}$  and  $a_{eq}$  values were obtained by substituting the  $P$ ,  $C_L$  and  $C_S$  values into Eqs. (12) and (13), respectively. The equivalent crack length corresponding to the initial crack length  $a_0$  was defined as  $a_{eq0}$ , and the propagation crack length  $\Delta a_{eq}$  was obtained as  $\Delta a_{eq} = a_{eq} - a_{eq0}$ . The  $G_{II}$ - $\Delta a_{eq0}$  relationships obtained by the beam theory and compliance combination methods were compared with each other.

In the compliance calibration method, the  $C_L$ - $a$  relationship was regressed into the following 4<sup>th</sup> polynomial function:

$$C_L = A_0 + A_1 a + A_2 a^2 + A_3 a^3 + A_4 a^4 \quad (14)$$

where  $A_0$ - $A_4$  are the parameters obtained by the regression. Using Eq. (14), the  $G_{II}$  value was derived as:

$$G_{II} = \frac{P^2}{2B} \frac{dC_L}{da} = \frac{P^2}{2B} (A_1 + 2A_2 a + 3A_3 a^2 + 4A_4 a^3) \quad (15)$$

In the compliance calibration method,  $\Delta a_{eq}$  was defined as  $a - a_0$ , and the obtained  $G_{II}$ - $\Delta a_{eq}$  relationship was compared with those obtained from the aforementioned data

reduction methods.

In several previous studies of 3ENF, ONF, and 4ENF tests [17-24], the compliance calibration was conducted by shifting a specimen in the support and virtually varying the crack length. Otherwise, the specimens with various crack lengths corresponding to the  $c/2L$  value should be prepared to obtain the  $C_L$ - $a$  relationship. In this study, however, it was difficult to prepare specimens that satisfied these conditions. In the actual 3EENF tests performed in this study, the compliance calibration method was not adopted for the data reduction.

The  $G_I$  and  $G_{II}$  values were also calculated using a virtual crack closure technique (VCCT) as follows [27]:

$$\begin{cases} G_I^{\text{VCCT}} = \frac{F_y^j d_y^i}{2BDa} \\ G_{II}^{\text{VCCT}} = \frac{F_x^j d_x^i}{2BDa} \end{cases} \quad (16)$$

where  $F_x^j$  and  $F_y^j$  are the nodal forces at the crack tip node  $j$  in the  $x$ - and  $y$ -directions, respectively, and  $\delta_x^i$  and  $\delta_y^i$  are the relative displacements of the nodes  $i$  and  $i'$ , which are located at a distance  $\Delta\alpha$  behind the crack tip, in the  $x$ - and  $y$ -directions, respectively.

Similar to the compliance calibration method,  $\Delta a_{\text{eq}}$  was defined as  $a - a_0$ , and the

obtained  $G_{II}-\Delta a_{eq}$  relationship was compared with the three data reduction methods.

## 4. Experiment

### 4.1. Materials

Western hemlock (*Tsuga heterophylla* Sarg.) lumber with a density of  $463 \pm 13$  kg/m<sup>3</sup> and eight or nine annual rings contained in a radial length of 10 mm was used for the tests. As shown in Fig. 4, the annual rings were sufficiently flat and their curvature could thus be ignored. The lumber contained no defects such as knots or grain distortions, and the specimens cut from it could be regarded as “small and clear.” Prior to the test, the lumber was stored for approximately one year in a room at a constant temperature of 20°C and a relative humidity of 65% and was confirmed to be in an air-dried condition. These conditions were maintained throughout the tests. After conducting the 3EENF test, the specimen was oven-dried for measuring the MC of the specimens, which were  $11.7 \pm 0.2\%$ . The Young’s modulus in the longitudinal direction,

which corresponds to  $E_x$ , was  $12.6 \pm 0.5$  GPa, as measured by the flexural vibration tests previously conducted by the 3EENF tests. The influence of shear deflection on the  $E_x$  value was reduced based on Timoshenko's vibration theory [28]. Five specimens were used for one test condition.

#### 4.3. Three-point eccentric end-notched flexure tests

All of the specimens were cut from the aforementioned lumber such that they were side-matched according to the dimensions of 430 mm (longitudinal direction)  $\times$  12 mm (tangential direction)  $\times$  24 mm (radial direction). As previously noted, the crack propagation must precede the bending failure in a fracture test. The bending stress is maximised at the point where  $x = a$  and is defined as  $\sigma_{m \square \square}$  and derived as follows:

$$S_{\max} = \frac{3(2L - c)Pa}{2BH^2L} \quad (17)$$

To allow the crack to propagate while preventing the bending failure, the load  $P$  satisfying Eq. (2) should be smaller than that satisfying Eq. (17). Therefore, the depth in the cracked portion  $H$  should satisfy the following inequality:

$$H > \frac{4E_x G_{\text{IIR}}}{S_{\text{max}}^2} \quad (18)$$

Equation (18) indicates that the critical value of  $H$  is independent of the location of the loading point  $c/2L$ . Based on the  $G_{\text{IIR}}$  and  $\sigma_{\text{max}}$  values, which were supposed to be approximately  $1000 \text{ J/m}^2$  and  $100 \text{ MPa}$ , the critical value of  $H$  was  $6.4 \text{ mm}$ . To firmly enhance the crack propagation while preventing the specimen from bending failure, the  $H$  value was determined as  $12 \text{ mm}$  in this study. In addition, the results of the FEAs indicated that the bending rotation at the supports is smaller than  $0.1 \text{ rad}$ , so the deformation was small enough not to consider the large bending in the 3EENF test.

The crack was produced in the longitudinal direction along the longitudinal-radial plane, which is the so-called RL-system. Therefore, the  $x$ - and  $y$ -directions correspond to the longitudinal and tangential directions of the wood. The crack was initially cut with a band saw (thickness =  $0.3 \text{ mm}$ ), and then extended ahead of the crack tip using a razor blade to the initial crack length  $a_0$  shown in Table 2. Straight lines were drawn perpendicular to the crack in the crack-free region at the intervals shown in Table 3 to observe the approximated location of the crack tip. Two sheets of  $0.05\text{-mm}$ -thick Teflon were inserted between the crack surfaces to reduce the friction between the upper and

lower cantilever beams. The specimen was supported by 400-mm spans. To prevent the specimen from indenting at the supporting point, a steel platen with a width of 30 mm was placed between the specimen and the supporting point. A load was applied to the point of  $x = c$  at a cross-head speed of 1 mm/min until the crack tip reached the straight line drawn below the loading point. Fig. 5 shows the set-up of the 3EENF test. The total testing time was approximately 15 min.

A displacement gauge was placed below the loading point to obtain the deflection at the loading point  $\delta$ . The longitudinal strain,  $\varepsilon_x$ , was measured using a strain gauge (gauge length = 2 mm; FLA-2-11, Tokyo Sokki Kenkyujo Co., Tokyo) that was bonded at a point behind the loading point. In the bending loading, the longitudinal strain varied in the length direction of the beam, and this variation may have affected the accuracy of the flexural Young's modulus value measured by the strain gauge. In addition, there was concern that a measurement error was induced because the output from the strain gauge was influenced by the pointwise material property variation at the region where the strain gauge was bonded [29]. However, these concerns were reduced with a homogeneous specimen and a short strain gauge [26, 30]. Recently, the digital image

correlation (DIC) technique is adopted for determining the Young's modulus in a cracked sample [31, 32]. Although the DIC technique is more complicated than bonding a strain gauge, it is effective to characterising the elastic properties of a cracked sample, which dominate the accuracy of the fracture mechanics properties. Comparisons between these methods are required for a further research.

Fig. 6 shows the typical  $P-\delta$  and  $P-\varepsilon_x$  relationships. Similar to several previous studies [9, 11, 23, 24], the initial load-deflection compliance  $C_{L0}$  and load-strain compliance  $C_S$  were determined from the initial slope of the  $P-\delta$  and  $P-\varepsilon_x$  relationships, respectively, whereas the temporary load-loading point deflection compliance  $C_L$  was determined from the slope of the straight line drawn in the nonlinear region of the  $P-\delta$  relationship. The equivalent crack length ( $a_{eq}$ ) and propagation fracture ( $G_{IIR}$ ) values during the crack propagation were obtained by substituting the  $P$ ,  $C_L$ , and  $C_S$  values into Eqs. (12) and (13), respectively. The critical load for crack propagation, defined as  $P_c$ , was determined as that at the onset of nonlinearity in the  $P-\delta$  relationship as shown in Fig. 6. The initiation fracture toughness  $G_{IIc}$  was obtained by substituting the  $P_c$ ,  $C_{L0}$ , and  $C_S$  values into Eq. (13). Similar to the FEM, the propagation crack length  $\Delta a_{eq}$  was

obtained as  $\Delta a_{eq} = a_{eq} - a_{eq0}$ , and the  $R$ -curve was obtained as the  $G_{IIR}-\Delta a_{eq}$  relationship.

In addition, the  $G_{IIR}$  values were averaged, and the representative value of propagation fracture toughness, defined as  $\overline{G_{IIR}}$ , was obtained. In this study, the plateau region of

the  $R$ -curve was defined as that between the maximal and minimal values of  $G_{IIR}$  before the continuous increasing of the  $G_{IIR}$  value, the details of which are described below.

The obtained  $G_{IIc}$  and  $\overline{G_{IIR}}$  values were compared with each other, and the effect of the loading location was examined.

## 5. Results and discussion

### 5.1. Finite element calculations

Fig. 7 shows the comparison of the relationships between the Mode II energy release rate  $G_{II}$  and propagation crack length  $\Delta a_{eq}$  obtained from the FEAs. In the VCCT, the total energy release rate (ERR) is defined as  $G^{VCCT} (= G_I^{VCCT} + G_{II}^{VCCT})$ , and the ratio of Mode II component to the total ERR,  $G_{II}^{VCCT}/G^{VCCT}$ , was larger than 99.9% for

all analysis results. Therefore, the 3EENF tests conducted in this study could be regarded to be a rather pure Mode II condition. All of the  $G_{II}$  values obtained by the data reduction methods and the VCCT were greater than  $1000 \text{ J/m}^2$ , which was obtained by substituting the  $a$  and  $P$  values listed in Table 3 into Eq. (2), because of the shear deformation and the crack tip rotation ahead of the crack tip [2-12]. The  $G_{II}$  values obtained from the beam theory and compliance combination methods were greater than those obtained from the VCCT. These discrepancies were enhanced as the  $c/2L$  value increased. In contrast, the  $G_{II}$  value obtained from the compliance calibration method, which was not adopted in the actual fracture test in this study, coincided well with that obtained from the VCCT.

There were discrepancies in the FEA results between the  $G_{II}$  values obtained from the different data reduction methods. In conventional 3ENF tests conducted in a previous study [5], however, these discrepancies were not so significant. In the FEAs conducted in this study, the softening behaviour due to the fracture process zone (FPZ) ahead of the crack tip was not taken into account, although it had been considered in the analyses of previously conducted 3ENF tests [6, 7, 34-37]. If the effect of the FPZ is

considered, then the FEA results may be different from those obtained in this study.

Further research should be conducted to reveal the validity of these data reduction methods in more detail.

Recently, Moutou Pitti et al. [38] adopted the  $M$ -integral for analysing the crack growth in orthotropic material like solid wood based on the approach by FEM. Although the  $M$ -integral is often complicated than the data reduction methods based on the compliance, they may be effective for characterising the fracture properties of solid wood. In addition, as described previously, there are several examples conducting the crack propagation simulations by FEA for characterising the fracture mechanics properties while the FPZ and fibre bridgings are taken into account [6, 7, 35-38]. Further researches are also required to examine the applicability of these novel methods on the 3EENF test.

## 5.2. Three-point end-notched flexure tests

Fig. 8 shows the  $R$ -curves obtained in the 3EENF tests under different loading

point locations. As shown in this figure, the crack wholly propagated stably during the test in the range of propagation crack length. It was revealed from the FEA and actual fracture test results that the  $G_{IIR}-\Delta a_{eq}$  relationships obtained from the beam theory and compliance combination methods coincided well with each other. Therefore, the  $R$ -curves in Fig. 7 were obtained based solely on the compliance combination method. Similar to the results shown in several previous studies, the  $R$ -curve initially increased steeply and then displayed a plateau region. After the plateau region, the  $R$ -curve increased again because of the concentration of stress around the loading point and the confinement of the FPZ [11, 36, 39]. In the conventional 3ENF test, the range of the  $l_s$  value was restricted because of the initial crack length, which should be longer than  $0.7L$ , and the confinement of the FPZ when the crack tip was close to the loading point. However, the range of  $\Delta a_{eq}$  in the  $R$ -curve can be extended by conducting the 3EENF test. Nevertheless, the  $G_{IIR}$  values in the plateau region of the specimens with  $c/2L$  values of 0.8 and 0.9 were often greater than the others. In addition, the variation of the  $G_{IIR}$  value was more significant in these conditions. As shown in the FEA results in Fig. 7, the greater  $G_{IIR}$  values in these conditions may be due to the compliance combination

method adopted in this study. In addition, the influence of the frictional force and fibre bridgings between the cracked surfaces may be significant for the  $R$ -curve behaviours of the specimens with  $c/2L$  values of 0.8 and 0.9, the cracked surfaces of which are relatively large. Therefore, the resistance against the crack propagation may be induced under these conditions. Further research should also be conducted to reveal these phenomena in more detail.

Fig. 9 shows the initiation and propagation fracture toughness values,  $G_{IIc}$  and  $\overline{G_{IIR}}$ , respectively, corresponding to the location of the loading point  $c/2L$ . The  $G_{IIc}$  values were constant independent of the  $c/2L$ . In contrast, the  $\overline{G_{IIR}}$  values of the specimens with  $c/2L = 0.8$  and  $0.9$  were significantly larger than the others, and the variation of the  $\overline{G_{IIR}}$  value was significant in these  $c/2L$  ranges. As demonstrated in several previous studies, Mode II fracture mechanics behaviours can be obtained from the conventional 3ENF test, where  $c/2L = 0.5$  [1-12]. Because the  $G_{IIc}$  and  $\overline{G_{IIR}}$  values in  $c/2L = 0.5-0.7$  are close to each other, the fracture mechanics properties obtained in these conditions are thought to be valid. In particular, the  $\Delta a_{eq}$  value is approximately twice as high in the condition of  $c/2L = 0.7$  than in the conventional 3ENF test condition

( $c/2L = 0.5$ ). In contrast, the 3EENF test conditions of  $c/2L = 0.8$  and  $0.9$  should be examined in more detail, although it is feasible to extend the propagation crack length under these conditions.

As described above, the sample behaves as if the crack length value is longer than the actual value because of the deformation caused by the transverse shear force, the FPZ, and the fibre bridgings. Considering this phenomenon, the  $\Delta$  value was evaluated from the following equation:

$$D = a_{\text{eq0}} - a_0 \quad (18)$$

Fig. 10 shows the  $\Delta$  value corresponding to the location of the loading point  $c/2L$ . The  $\Delta$  value was approximately 35 mm. Morel et al. pointed out that the length of the FPZ reaches approximately several centimetres [39]. The  $\Delta$  value contains the effects of deformation caused by the transverse shear force and the fibre bridgings as well as the FPZ, so it may not be comparable to the results obtained by Morel et al. As described above, however, it is reasonable that the large part of the  $\Delta$  value is because of the length of the FPZ, which induces the increase of the  $R$ -curve at the end of the fracture test.

## 6. Conclusions

Three-point end-notched flexure (3EENF) tests were conducted using specimens of western hemlock to determine the Mode II fracture mechanics properties, including the resistance curve (*R*-curve), initiation fracture toughness, and propagation fracture toughness. These properties were obtained using a compliance combination method as the data reduction method. In addition to the fracture tests, finite element analyses (FEAs) were conducted and the validity of the 3EENF test methods were also examined.

The FEA results demonstrated that the discrepancies of the  $G_{II}$  values obtained from the data reduction methods (beam theory and compliance combination methods) and those obtained from the VCCT were more pronounced when the loading point approached the supporting point at the crack-free region.

For all of the specimens, the *R*-curve initially increased steeply, then displayed a plateau region, and finally increased again due to the concentration of stress around the

loading point and the confinement of the FPZ. The initiation fracture toughness  $G_{IIc}$  was not dependent on the location of the loading point. In contrast, the  $G_{IIR}$  values in the plateau region of the tests under the  $c/2L$  conditions of 0.8 and 0.9 were often greater than those under the  $c/2L$  conditions of 0.5-0.7. This phenomenon affected the represented value of propagation fracture toughness  $\overline{G_{IIR}}$ , which demonstrated a tendency similar to that of  $G_{IIR}$ .

Based on the summarized results obtained in this study, fracture mechanics properties can be appropriately obtained from a 3EENF test when the loading point is not extremely close to the supporting point at the crack-free region.

*Acknowledgments:* This work was supported in part by a Grant-in-Aid for Scientific Research (C) (No. 24580246) of the Japan Society for the Promotion of Science.

## **References**

[1] Barrett JD, Foschi RO. Mode II stress-intensity factors for cracked wood beams.

- Engrg Fract Mech 1977; 9: 371-8.
- [2] Yoshihara H, Ohta M. Measurement of mode II fracture toughness of wood by the end-notched flexure test. J Wood Sci 2000; 46: 273-8.
- [3] Yoshihara H. Influence of span/depth ratio on the measurement of mode II fracture toughness of wood by end-notched flexure test. J Wood Sci 2001; 47: 8-12.
- [4] Yoshihara H. Resistance curve for the mode II fracture toughness of wood obtained by end-notched flexure test under the constant loading point displacement condition. J Wood Sci 2003; 49 (3): 210-5.
- [5] Yoshihara H. Mode II initiation fracture toughness analysis for wood obtained by 3-ENF test. Compos Sci Technol 2005; 65: 2198-207.
- [6] Silva MAL, de Moura MFSF, Morais JJJ. Numerical analysis of the ENF test for mode II wood fracture. Composites A 2006; 37: 1334-44.
- [7] de Moura MFSF, Silva MAL, de Morais AB, Morais JJJ. Equivalent crack based mode II fracture characterization of wood. Engrg Fract Mech 2006; 73: 978-93.
- [8] de Moura MFSF, Silva MAL, Morais JJJ, de Morais AB, Lousada JJJ. Data reduction scheme for measuring  $G_{IIc}$  of wood in end-notched flexure (ENF) tests.

Holzforschung 2009; 63: 99-106.

- [9] Yoshihara H, Satoh A. Shear and crack tip deformation correction for the double cantilever beam and three-point end-notched flexure specimens for mode I and mode II fracture toughness measurement of wood. *Engrg Fract Mech* 2009; 76: 335-46.
- [10] Arrese A, Carbajal N, Vargas G, Mujika F. A new method for determining mode II *R*-curve by the end-notched flexure test. *Engrg Fract Mech* 2010; 77: 51-70.
- [11] Yoshihara H. Initiation and propagation fracture toughness of solid wood under the mixed Mode I/II condition examined by mixed-mode bending test. *Engrg Fract Mech* 2013; 104: 1-15.
- [12] Rhême M, Botsis J, Cugnoni J, Navi P. Influence of the moisture content on the fracture characteristics of welded wood joint. Part 2: Mode II fracture. *Holzforschung* 2013; 67: 755-61.
- [13] Kageyama K, Kikuchi M, Yanagisawa N. Stabilized end notched flexure test. Characterization of mode II interlaminar crack growth. *ASTM STP 1110* 1992: 210-25.
- [14] Davies P, Sims GD, Blackman BRK, Brunner AJ, Kageyama K, Hojo M, Tanaka K,

- Murri G, Rousseau C, Gieseke B, Martin RH. Comparison of test configuration for the determination of  $G_{IIc}$ : Results from an international round robin. *Plast Rubber Compos* 1999; 28: 432-7.
- [15] Silva MAL, Morais JIL, de Moura MFSF, Lousada JL. Mode II wood fracture characterization using the ELS test. *Engrg Fract Mech* 2007; 74: 2133-47.
- [16] Qiao PZ, Wang JL, Davalos JF. Analysis of tapered ENF specimen and characterization of bonded interface fracture under Mode-II loading. *Int J Solid Struct* 2003; 40: 1865-84.
- [17] Wang J, Qiao PZ. Novel beam analysis of end notched flexure specimen for mode-II fracture. *Eng Fract Mech* 2004; 71: 219-31.
- [18] Kutnar A, Kamke FA, Nairn JA, Senek M. Mode II fracture behavior of bonded viscoelastic thermal compressed wood. *Wood Fiber Sci* 2008; 40: 362-73.
- [19] Wang WX, Nakata M, Takao Y, Matsubara T. Experimental investigation on test methods for mode II interlaminar fracture testing of carbon fiber reinforced composites. *Composites A*. 2009; 40: 1447-55.
- [20] Martin RH, Davidson BD. Mode II fracture toughness evaluation using four point

- bend, end notched flexure test. *Plast Rubber Compos.* 1999; 28: 401–6.
- [21] Schuecker C, Davidson BD. Evaluation of the accuracy of the four-point bend end-notched flexure test for mode II delamination toughness determination. *Compos Sci Technol.* 2000; 60: 2137-46.
- [22] Davidson BD, Sun X. Effects of friction, geometry, and fixture compliance on the perceived toughness from three-and four-Point bend end-notched flexure tests. *J Reinforced Plast Compos* 2005; 24: 1611-28.
- [23] Yoshihara H. Mode II *R*-curve of wood measured by 4-ENF test. *Eng Fract Mech* 2004; 71: 2065-7.
- [24] Yoshihara H. Theoretical analysis of 4-ENF tests for mode II fracturing in wood by finite element method. *Engrg Fract Mech* 2008; 75: 290-296.
- [25] Qiao P, Zhang L, Chen F, Chen Y, Shan L. Fracture characterization of Carbon fiber-reinforced polymer-concrete bonded interfaces under four-point bending. *Engrg Fract Mech* 2011; 78: 1247-63.
- [26] Yoshihara H, Kubojima Y, Ishimoto T. Several examinations on the static bending test methods of wood using todomatsu (Japanese fir). *Forest Prod J* 2003; 52(2):

39-44.

[27] Krueger R. The virtual crack closure technique: History, approach and applications.

NASA CR-2002-211628; 2002.

[28] Yoshihara H. Examination of the specimen configuration and analysis method in the flexural and longitudinal vibration tests of solid wood and wood-based materials. *Forest Prod J* 2012; 62(3): 191-200.

[29] Yadama V, Davalos JF, Loferski JR, Holzer SM. Selecting a gauge length to measure parallel-to-grain strain in southern pine. *Forest Prod J* 1991; 41(10): 65-8.

[30] Yoshihara H, Tsunematsu S. Feasibility of estimation methods for measuring Young's modulus of wood by three-point bending test. *Mater Struct* 2006; 39: 29-36.

[31] Dubois F, Méité M, Pop O, Absi J. Characterization of timber fracture using the Digital Image Correlation technique and Finite Element Method. *Engrg Fract Mech* 2012; 96: 107-21.

[32] Méité M, Pop O, Dubois F, Absi J. Characterization of mixed-mode fracture based on a complementary analysis by means of full-field optical and finite element

approaches. *Int J Fract* 2013; 180: 41-52.

[33] Morel S, Lespine C, Coureau JL, Planas J, Dourado N. Bilinear softening parameters and equivalent LEFM R-curve in quasibrittle failure. *Int J Solid Struct* 2010; 47: 837-50.

[34] Dourado N, Morel S, de Moura MFSF, Valentin G, Morais J. Comparison of fracture properties of two wood species through cohesive crack simulations. *Composites A* 2008; 39: 415-27.

[35] Dourado N, Morel S, de Moura MFSF, Valentin G, Morais J. A new data reduction scheme for mode I wood fracture characterization using the double cantilever beam test. *Engrg Fract Mech* 2008; 75: 3852-65.

[36] de Moura MFSF, Dourado N, Morais JLL, Pereira FAM. Numerical analysis of the ENF and ELS tests applied to mode II fracture characterization of cortical bone tissue. *Fatigue Fract Engrg Mater Struct* 2011; 34: 149-58.

[37] Lartigau J, Coureau JL, Morel S, Galimard P, Maurin E. Mixed mode fracture of glued-in rods in timber structures. A new approach based on equivalent LEFM. *Int J Fract* 2014; in press (online available).

[38] Moutou Pitti R, Dubois F, Petit C, Sauvat N, Pop O. A new  $M$ -integral parameter for mixed-mode crack growth in orthotropic viscoelastic material. *Engrg Fract Mech* 2008; 75: 4450-65.

[39] Coureau JL, Morel S, Dourado N. Cohesive zone model and quasibrittle failure of wood: A new light on the adapted specimen geometries for fracture tests. *Engrg Fract Mech* 2013; 109: 328-40.

## Figure captions

Fig. 1. Schematic diagram of the three-point eccentric end-notched flexure (3EENF) test.

Fig. 2. Relationship between the  $l_s/2L$  and  $c/2L$  values.

Fig. 3. The finite element (FE) meshes used in the simulations. Unit = mm.  $a$  and  $P$  values corresponding to the length between the left supporting point and loading point  $c$  are listed in Table 3.

Fig. 4. Photograph of cross-section of the material used in this experiment

Fig. 5. Set-up of the three-point end-notched flexure (3EENF) test.

Fig. 6. Load-deflection at the loading point, load-longitudinal strain relationships and the definitions of critical load for crack propagation  $P_c$ , temporary load-loading point deflection compliance  $C_L$ , initial load-loading point deflection compliance  $C_{L0}$ , and load-longitudinal strain compliance  $C_S$ .

Fig. 7. Relationships between the Mode II energy release rate  $G_{II}$  and propagation crack length  $\Delta a_{eq}$  obtained from the FEAs.

Fig. 8. Resistance curves ( $R$ -curves) obtained in the 3EENF tests under different loading locations. Data reduction was conducted based on the compliance combination method.

Fig. 9. Initiation and representative propagation fracture toughness values,  $G_{IIc}$  and  $\overline{G_{IIR}}$ , respectively, corresponding to the location of the loading point  $c/2L$ . The results are the average  $\pm$  SD.

Fig. 10. Correction value of crack length calculated from the compliance combination method  $\Delta$  corresponding to the location of the loading point  $c/2L$ . The results are the average  $\pm$  SD.

Table 1. Elastic constants used for the finite element analysis and data reduction.

$E_x$ (GPa)	$E_y$ (GPa)	$G_{xy}$ (GPa)	$\nu_{xy}$
$16.0 \pm 0.8$	$0.73 \pm 0.10$	$0.61 \pm 0.04$	0.49

Results are the average  $\pm$  SD.  $x$ - and  $y$ -directions correspond to the longitudinal and tangential directions of sitka spruce data obtained in a previous study [10].

Table 2. The distance between the loading point and left supporting point,  $c$ , the maximum length for stabilising the crack propagation,  $l_s$ , and initial crack length  $a_0$  corresponding to the location of the loading point,  $c/2L$ .

$c/2L$	$c$ (mm)	$l_s/2L$	$l_s$ (mm)	$a_0$ (mm)
0.5	200	0.153	61	139
0.6	240	0.209	84	156
0.7	280	0.266	106	174
0.8	320	0.326	130	190
0.9	360	0.387	155	205

$a_0$  was determined as  $c - l_s$ .

Table 3. Applied load  $P$  corresponding to the crack length  $a$  in the FEAs.

$c = 200$ mm		$c = 240$ mm		$c = 280$ mm		$c = 320$ mm		$c = 360$ mm	
$a$ (mm)	$P$ (N)								
139	605	156	674	174	806	190	1107	205	2052
151	556	173	609	195	718	216	974	236	1782
163	515	190	555	216	648	242	869	267	1575
176	479	206	510	238	590	268	785	298	1412
188	448	223	471	259	542	294	715	329	1279
200	421	240	438	280	501	320	657	360	1168

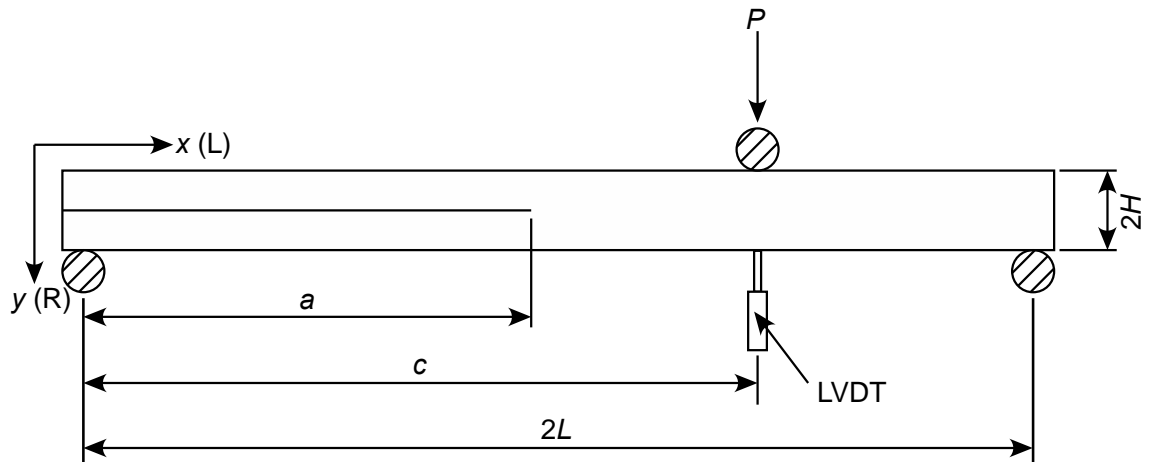


Fig. 1. Schematic diagram of the three-point eccentric end-notched flexure (3EENF) test.

L and R represent the longitudinal and radial directions, respectively.

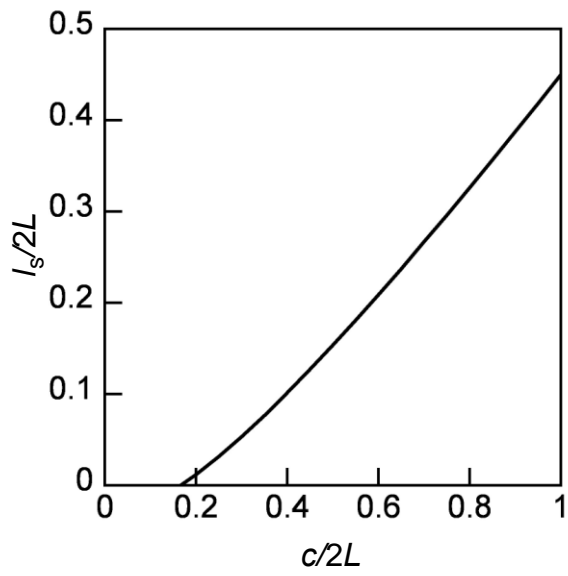
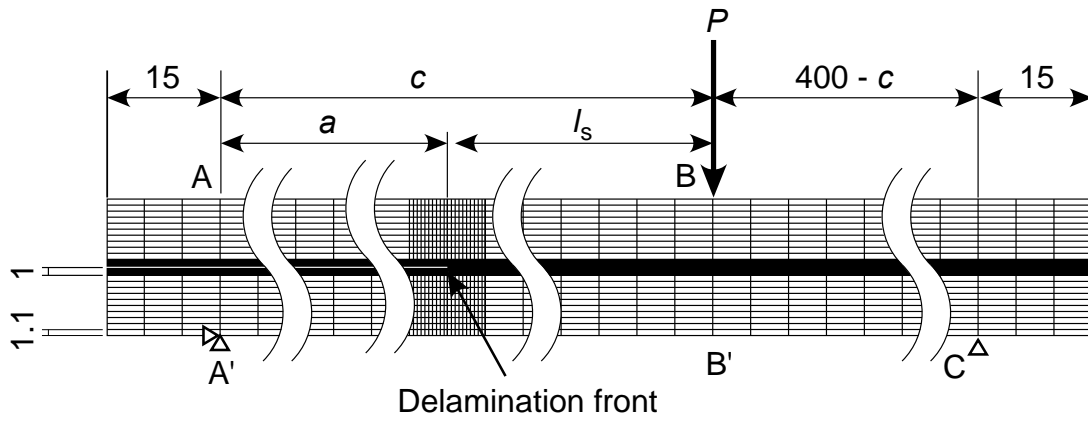
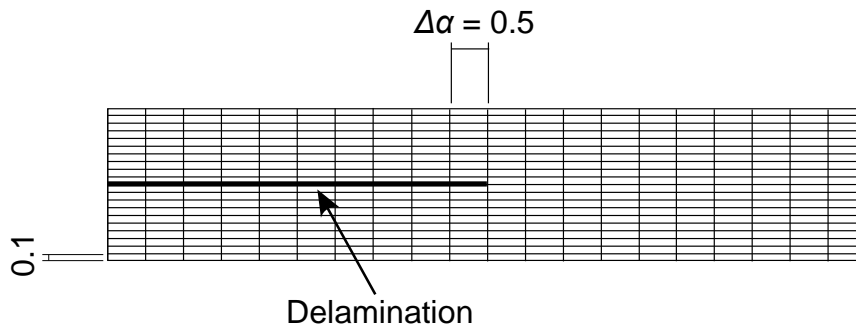


Fig. 2. Relationship between the  $l_s/2L$  and  $c/2L$  values.



(a) Whole mesh of 3EENF test simulation



(b) Detail around the delamination front

Fig. 3. The finite element (FE) meshes used in the simulations. Unit = mm.  $a$  and  $P$  values corresponding to the length between the left supporting point and loading point  $c$  are listed in Table 3.

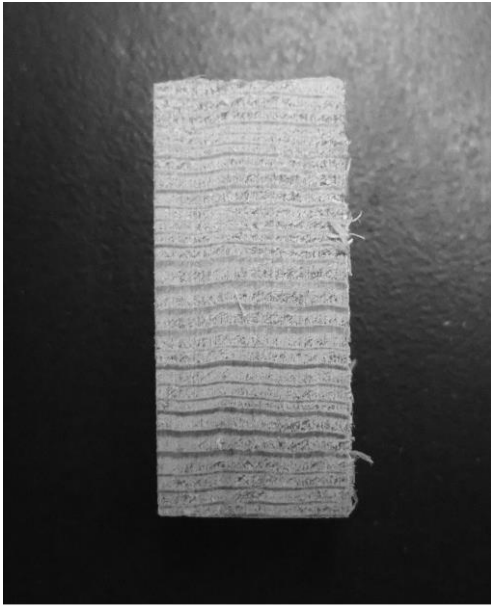


Fig. 4. Photograph of cross-section of the material used in this experiment

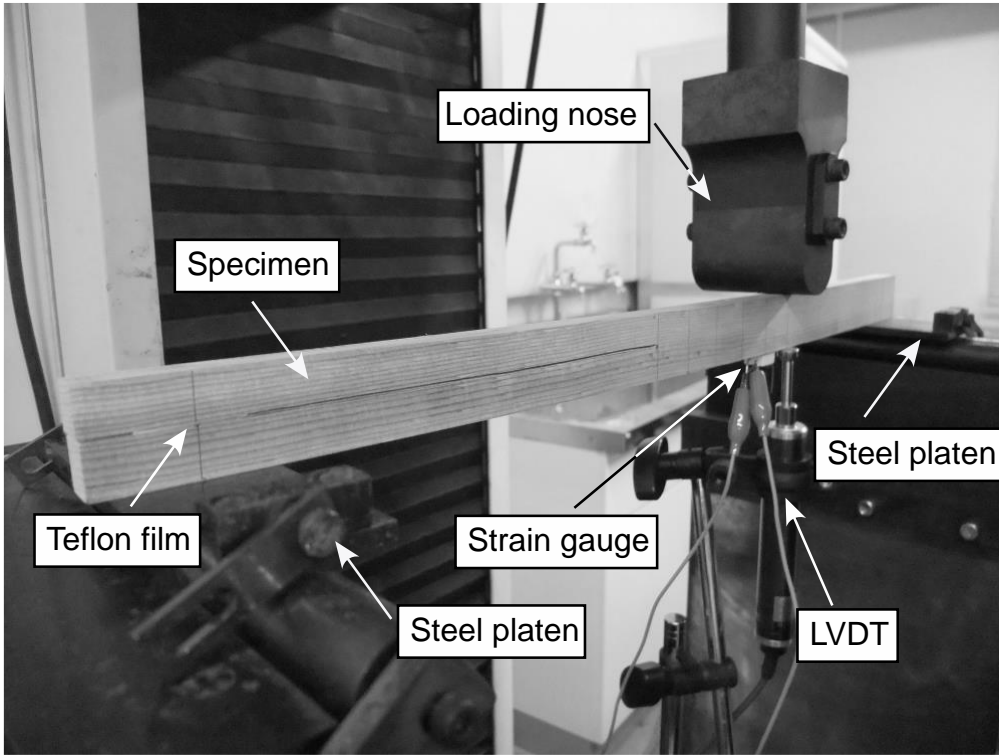


Fig. 5. Set-up of the three-point end-notched flexure (3EENF) test.

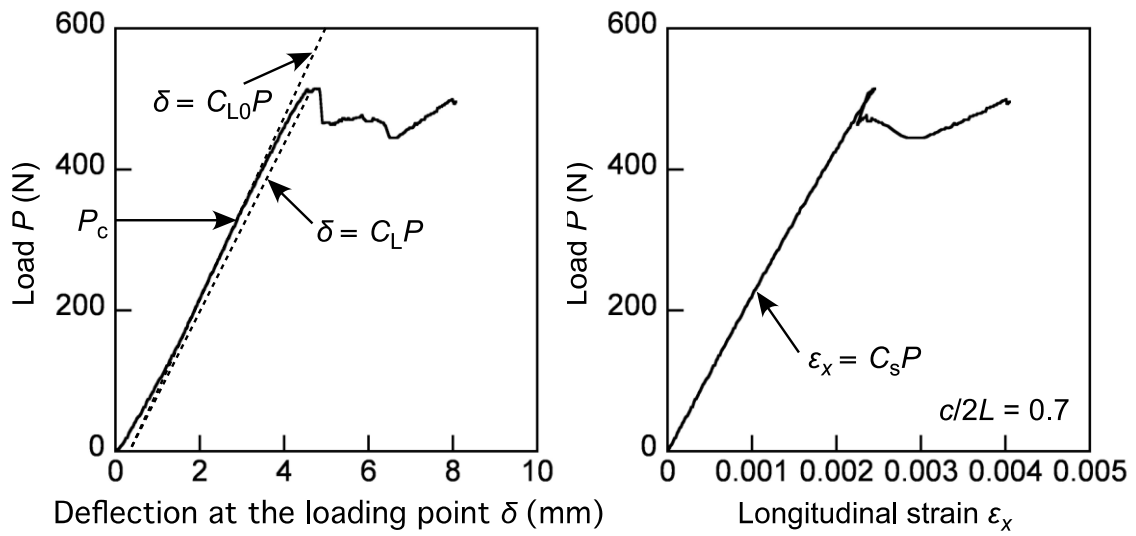


Fig. 6. Load-deflection at the loading point, load-longitudinal strain relationships and the definitions of critical load for crack propagation  $P_c$ , temporary load-loading point deflection compliance  $C_L$ , initial load-loading point deflection compliance  $C_{L0}$ , and load-longitudinal strain compliance  $C_s$ .

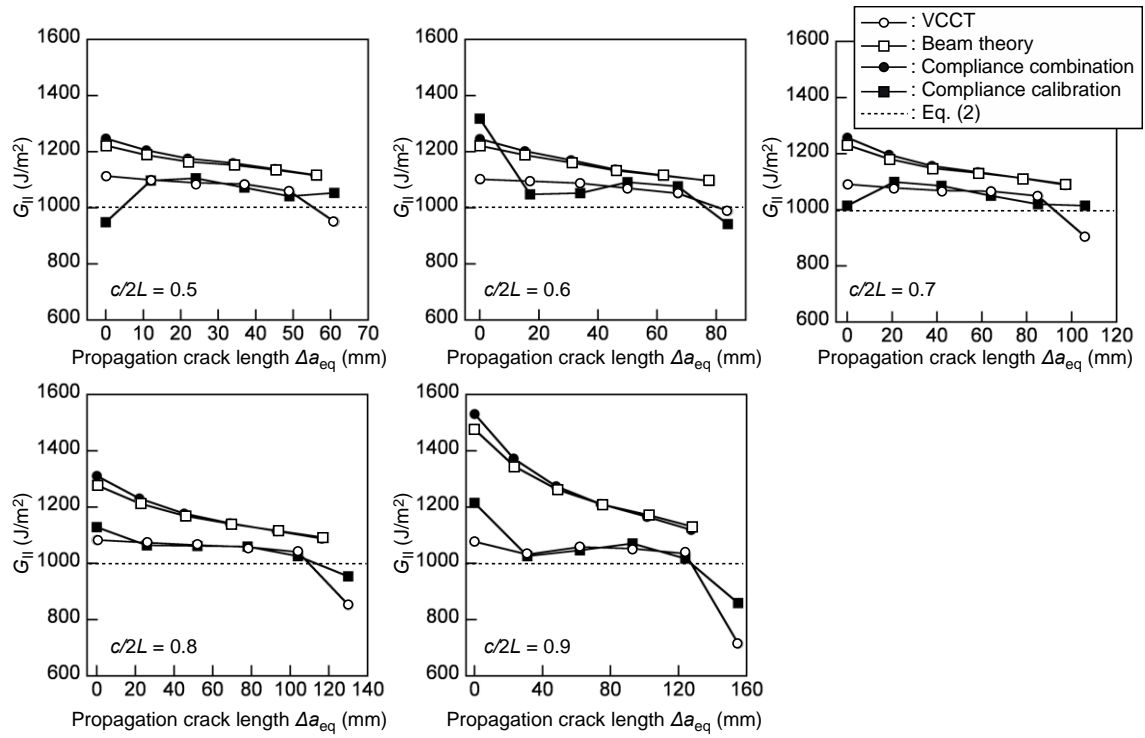


Fig. 7. Relationships between the Mode II energy release rate  $G_{II}$  and propagation crack length  $\Delta a_{eq}$  obtained from the FEAs.

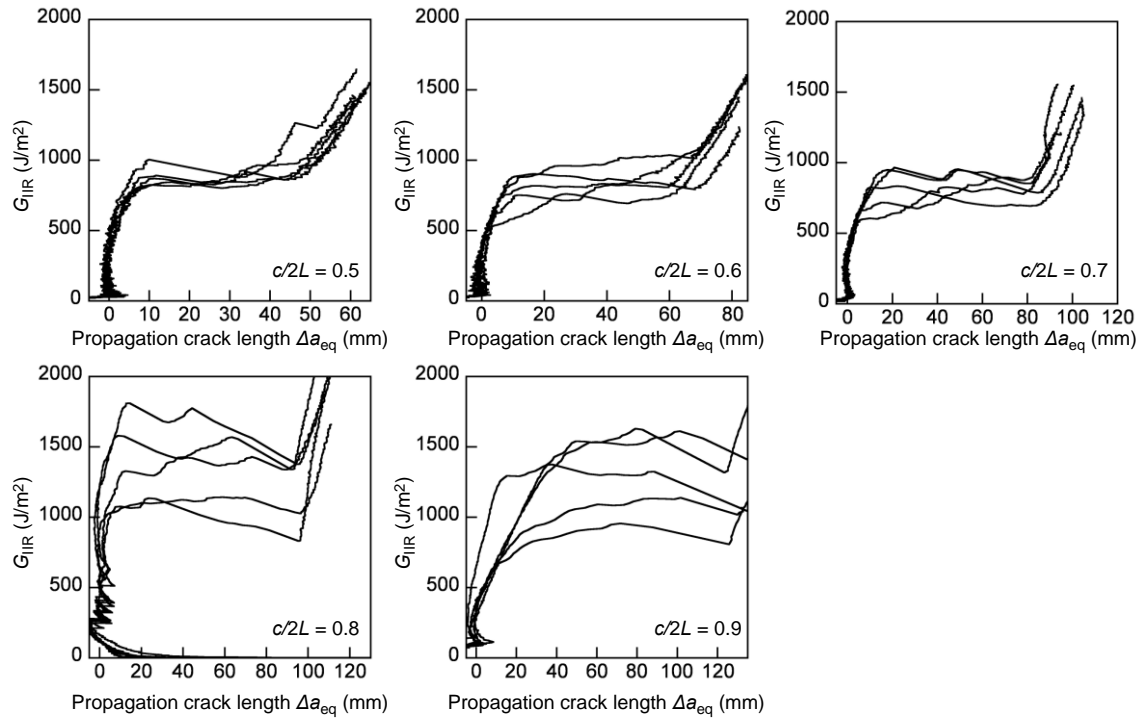


Fig. 8. Resistance curves ( $R$ -curves) obtained in the 3EENF tests under different loading locations. Data reduction was conducted based on the compliance combination method.

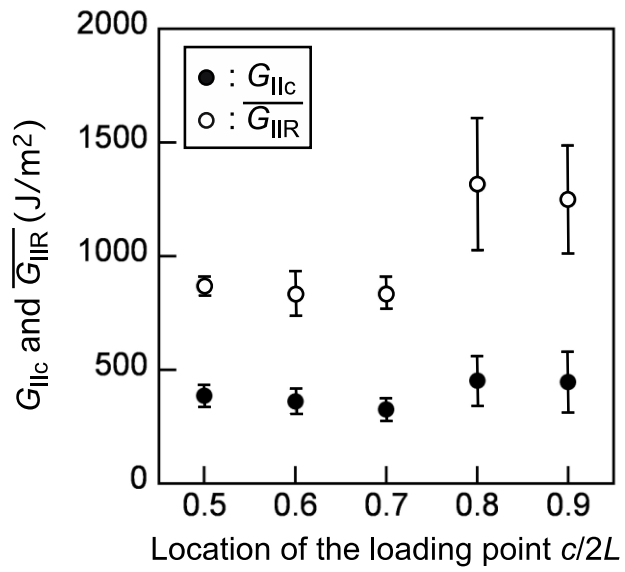


Fig. 9. Initiation and representative propagation fracture toughness values,  $G_{IIc}$  and  $\overline{G_{IIR}}$ , respectively, corresponding to the location of the loading point  $c/2L$ . The results are the average  $\pm$  SD.

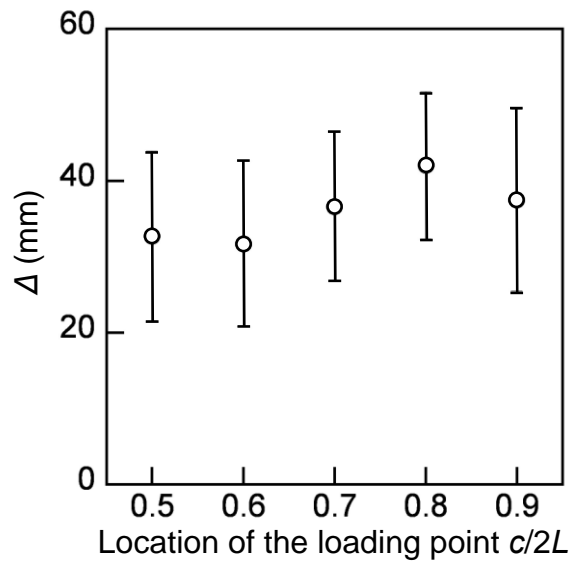


Fig. 10. Correction value of crack length calculated from the compliance combination method  $\Delta$  corresponding to the location of the loading point  $c/2L$ . The results are the average  $\pm$  SD.